Ocean Sci. Discuss., 11, 2205–2243, 2014
www.ocean-sci-discuss.net/11/2205/2014/
doi:10.5194/osd-11-2205-2014

Ocean Science
Discussions
Open Access

Circulation, eddies, oxygen and nutrient changes in the eastern tropical South Pacific Ocean

R. Czeschel[1], **L. Stramma**[1], **R. A. Weller**[2], **and T. Fischer**[1]

[1]Helmholtz Centre for Ocean Research Kiel (GEOMAR), Düsternbrooker Weg 20, 24105 Kiel, Germany
[2]Woods Hole Oceanographic Institution (WHOI), 266 Woods Hole Rd, Woods Hole, MA, 02543, USA

Received: 1 September 2014 – Accepted: 8 September 2014 – Published: 23 September 2014

Correspondence to: R. Czeschel (rczeschel@geomar.de)

Published by Copernicus Publications on behalf of the European Geosciences Union.

Abstract

A large, subsurface oxygen deficiency zone is located in the eastern tropical South Pacific Ocean (ETSP). The large-scale circulation in the eastern equatorial Pacific and off Peru in November/December 2012 shows the influence of the equatorial current system, the eastern boundary currents, and the northern reaches of the subtropical gyre. In November 2012 the Equatorial Undercurrent is centered at 250 m depth, deeper than in earlier observations. In December 2012 the equatorial water is transported southeastward near the shelf in the Peru-Chile Undercurrent with a mean transport of 1.6 Sv. In the oxygen minimum zone (OMZ) the flow is overlaid with strong eddy activity on the poleward side of the OMZ. Floats with parking depth at 400 m show fast westward flow in the mid-depth equatorial channel and sluggish flow in the OMZ. Floats with oxygen sensors clearly show the passage of eddies with oxygen anomalies. The long-term float observations in the upper ocean lead to a net community production estimate at about 18° S of up to 16.7 mmol C m^{-3} yr^{-1} extrapolated to an annual rate and 7.7 mmol C m^{-3} yr^{-1} for the time period below the mixed layer. Oxygen differences between repeated ship sections are influenced by the Interdecadal Pacific Oscillation, by the phase of El Niño, by seasonal changes, and by eddies and hence have to be interpreted with care. At and south of the equator the decrease in oxygen in the upper ocean since 1976 is related to an increase in nitrate, phosphate, and in part in silicate.

1 Introduction

The circulation in the eastern tropical South Pacific is still not well described. For the upper ocean some schematic circulation schemes have been developed (e.g. Kessler, 2006; Ayon et al., 2008; Grasse et al., 2012); however, information on the mid-depth circulation below 100 m depth is sparse due to the limited number of direct observations.

OSD
11, 2205–2243, 2014

The flow field in the eastern South Pacific is dominated by the Peru-Chile Current System (PCCS), also called the Humboldt Current System (HCS). In the equatorial Pacific, a complicated set of zonal currents exists which at 95° W in October–November 2003 have speeds of up to 0.9 m s^{-1} for the eastward flowing Equatorial Undercurrent (EUC) and are described as major supply paths of oxygen to the oxygen minimum zones (OMZs) (Stramma et al., 2010). In the eastern Pacific, the equatorial currents weaken in part because of the presence of the Galapagos Islands at the equator (Karnauskas et al., 2010). The most important and best investigated equatorial currents include the westward flowing South Equatorial Current (SEC), with a northern band north of the equator (SEC(N)) and southern bands south of the equator (SEC(S)), the eastward flowing North and South Equatorial Countercurrents (NECC, SECC) at and below the surface, and the EUC as well as the Northern and Southern Subsurface Countercurrents (NSCC, SSCC) below about 50 m depth. The NSCC and SSCC start around 3° from the equator in the western Pacific, then gradually diverge and shoal to the east, with cores around 6° from the equator and 150 m below the surface by 110° W (Rowe et al., 2000). Another eastward current, the secondary SSCC (sSSCC) is found poleward of the SSCC and extends to greater densities (Rowe et al., 2000). Firing et al. (1998) described a westward South Equatorial Intermediate Current (SEIC) and a North Equatorial Intermediate Current (NEIC) centered around 500 m and 3° from the equator. A westward Equatorial Intermediate Current (EIC) is often found below the EUC in the western Pacific (Firing et al., 1998). In February 2009 the NEIC and the EIC could hardly be separated into an off (north) and equatorial branch (Czeschel et al., 2011). Even deeper, denser, and weaker eastward current extremes (North and South Intermediate Countercurrents; SICC, NICC) are found at about 2° from the equator from 500 to 1500 m (Firing et al., 1998).

The coastal geometry connects regions of coastal and equatorial upwelling in the eastern Pacific Ocean. This connection extends to the subsurface Peru-Chile Undercurrent (PCUC) and the surface Peru-Chile Countercurrent; both are in part fed by the EUC. The subtropical gyre of the South Pacific Ocean contributes to several current

OSD
11, 2205–2243, 2014

bands of the SEC. Near the shelf it contributes to the Peru Coastal Current and the Peru Oceanic Current which flow equatorward in near surface layers close to the coast and further than ∼ 150 km from the coast, respectively, and to a deep equatorward current, referred to as the Chile-Peru Deep Coastal Current, flowing below the PCUC (Chaigneau et al., 2013).

From a large-scale hydrographic survey in February 2009, Czeschel et al. (2011) described the large-scale mid-depth circulation off Peru for the region of the oxygen minimum zone (OMZ) at 400 m depth, including comparison to model results and discussion of the spreading paths of floats. As the mean currents are weak, eddy variability dominates the flow and the supply of oxygen to the OMZ (Czeschel et al., 2011). During the last two decades eddies have been recognized to play an important role in the vertical and horizontal transport of momentum, heat, mass and the chemical constituents of seawater, such as oxygen and nutrients (e.g. Klein and Lapeyre, 2009). Three types of eddies have been identified: cyclonic, anticyclonic and mode water eddies (e.g. McGillicuddy Jr. et al., 2007). Data from a cruise in November 2012 have been used to describe the nutrient distribution in eddies off the shelf of Southern Peru (Stramma et al., 2013). Close to the equator hardly any eddies are seen in sea surface height anomaly satellite data, in part due to technical difficulties, while off the southern coast of Peru many cyclonic and anticyclonic eddies are observable (Chelton et al., 2011). The eddy frequency off Peru at 15 to 18° S reaches up to 50 % (Chaigneau et al., 2008). At the Stratus mooring (∼ 20° S, 85° W) about 1000 km off the South American continent a strong mode water eddy was observed which formed 11 months earlier off the Chilean shelf (Stramma et al., 2014).

Profiling floats are ideal tools for continuous sampling of the ocean instead of short-time measurements from ships. Besides CTD profiles, additional parameters can be measured, including oxygen. Floats with oxygen sensors were used in the past to investigate the net production of oxygen in the subtropical ocean (Riser and Johnson, 2008), to describe the oxygen distribution on a float drifting from Chile to Peru (Ulloa

OSD
11, 2205–2243, 2014

et al., 2012), and to collect oxygen time series to investigate oxygen trends (Czeschel et al., 2012).

Long-term oxygen trends were observed in the equatorial Pacific (e.g. Stramma et al., 2010) which are overlaid by climate-forced variations like El Niño and the Pacific Decadal Oscillation (Deutsch et al., 2011). Based on model results, the decadal and bidecadal climate variability in the tropical Pacific is controlled by the off-equatorial South Pacific Ocean (Tatebe et al., 2013). Hence, a comparison of recent measurements with earlier surveys might help to find out whether the model derived climate connections are visible in observations.

Here we will use the hydrographic data from an open ocean cruise leg in November 2012 and a near-shelf leg in December 2012 to investigate the large-scale circulation in subsurface layers of the eastern tropical South Pacific. These results will be compared to sections from earlier cruises and to float data to better define the large scale circulation and to describe changes and trends in the circulation and parameter distributions. In addition, float data will be used to describe the passage of eddies and to provide a net community production estimate for the eastern South Pacific. The aim of this investigation is to better understand the flow field with its variability on different time-scales and with changes caused by eddies and thus to better understand the existing shape of the OMZ in the eastern tropical South Pacific and its changes with time.

2 The data set

Cruises M90 and M91 on the German research vessel R/V *Meteor* took place in November and December 2012 to investigate the factors controlling the intensity and areal extent of the OMZ of the eastern tropical Pacific Ocean. The cruise M90 started in Cristobal, Panama, on 29 October and ended on 28 November 2012 in Callao, Peru. Cruise M91 started in Callao, Peru on 1 December 2012. Several sections perpendicular to the shelf and parallel to the shelf were carried out from north to south between 5

OSD
11, 2205–2243, 2014

and 16° S (Fig. 1). The cruise ended again in Callao on 26 December 2012. From 2° N, 85°50′ W on 1 November to 24° S, 88° W on 13 November a former World Ocean Circulation Experiment section along 85°50′–88° W (WOCE section P19) was reoccupied; this section had been sampled in late March 1993 on R/V *Knorr* with the northernmost station used here occupied during the R/V *Knorr* cruise on 1 April 1993. This section, called the 86° W section in the following, is located at 85°50′ W between 2° N and 15°07′ S and shifts to 88° W between 15°07′ and 20° S. The 86° W section had been sampled already on a cruise with R/V *Meteor* (*Meteor* cruise M77/4 from Callao 27 January to Panama 18 February 2009) between 14° S on 1 February 2009 and 2° N on 16 February 2009. A section along 6° S east of 85°50′ W sampled in February 2009 was reoccupied. Starting on 15 November 2012 another former WOCE section along 16°45′ S sampled in April 1994 was reoccupied by following an eastward cruise track from 87° W to the coast of Peru (Fig. 1). On the basis of satellite sea level height anomaly images forwarded to the ship, several eddies were identified in the area. A detailed survey of two major anticyclonic eddies and one cyclonic eddy along the 16°45′ S section including acoustic Doppler current profiling (ADCP), measurements of conductivity/temperature/depth (CTD), and of major biogeochemical parameters (O_2, nutrients, chlorophyll, and turbidity) along several additional subsections across the eddies had been performed in an earlier study (Stramma et al., 2013).

Two ADCP systems recorded the ocean velocities in November/December 2012: a hull mounted RDI OceanSurveyor 75 kHz ADCP provided the velocity distribution to about 700 m depth, while a 38 kHz ADCP mounted in the sea-well provided velocity profiles down to about 1200 m depth. As this investigation is on the upper ocean the data shown in this study are exclusively from the 75 kHz ADCP, which has a higher resolution in the upper ocean. For the R/V *Meteor* cruise in February 2009 only the 75 kHz ADCP was available. The shipboard ADCP on the R/V *Knorr* 1993 cruise reached a maximum depth of 493 m. Lowered ADCP data were collected north of 5° S in March 1993 and are used here to extend the vertical range of shipboard ADCP data of the R/V *Knorr* 1993 cruise.

OSD
11, 2205–2243, 2014

A Seabird CTD system with a General Oceanics rosette with 24 10 L-water bottles was used for water profiling and discrete water sampling on both cruises. The CTD system was used with double sensors for temperature, conductivity (salinity) and oxygen. The CTD oxygen sensors were calibrated with oxygen measurements obtained from discrete samples from the rosette applying the classical Winkler titration method, using a non-electronic titration stand (Winkler, 1888; Hansen, 1999). The precision of the oxygen titration determined during cruise M90 in November 2012 was ±0.45 µmol L^{-1}. The uncertainty of the CTD oxygen sensor calibration was determined as a r.m.s. of ±0.68 µmol kg^{-1}. However, with the classical titration method we were not able to determine oxygen concentrations below about 2 µmol kg^{-1} and hence oxygen concentrations below about 2 µmol kg^{-1} could not be measured with the CTD oxygen sensors as well.

The oxygen background fields were taken from the CSIRO Atlas of Regional Seas (CARS) 2009 digital climatology (Ridgway et al., 2002), for the November values above 400 m depth and the annual mean below 400 m depth.

Aviso satellite derived altimeter sea surface height anomaly data (SSHA) were used to define the general background distribution of the circulation and eddies. The SSHA data used in this study are delayed time products and combine available data of all satellites. The data are resampled on a regular 0.25° × 0.25° grid and are calculated with respect to a seven-year mean (http://www.aviso.oceanobs.com).

In the framework of the VOCALS project (Mechoso et al., 2014) 10 floats with Seabird SBE 43 oxygen sensors integrated into a SBE41CP CTD were deployed in October 2008 at about 20° S between 75 and 85° W. Six of the floats failed within the first months; however, four floats provided good oxygen time series until February 2014 with an initial cycling interval of 3 days in the upper 600 to 800 m depth. After about 11 months the cycling interval was increased to 10 days.

Ten profiling floats with Aanderaa oxygen sensors from the German research initiative SFB-754 were deployed in February 2009 along the 85°50′ W section, in pairs at 10, 8, 6, 4 and 2° S; one of each pair had a parking depth of 400 dbar and the

OSD
11, 2205–2243, 2014

other 1000 dbar. An additional 8 floats with Aanderaa oxygen sensors were deployed in April 2011 along 20° S at 75.58, 76.49, 77.01 and 85.68° W. These floats were again deployed in pairs with drifting depths at 400 and 1000 dbar, and cycling intervals of 10 days. Satellite data were used during the 2011 cruise to find eddy features and deploy the floats in eddies. The shallow parking depth of our floats is a particular difference compared to most floats of other groups, which have parking depths of about 1000 and 1500 m and can be used to describe the flow field in these depths layers (e.g. Cravatte et al., 2012). The floats drifting at 400 dbar were particularly aimed to analyze their spreading behavior near the core of the OMZ of the eastern Pacific.

3 Results

3.1 The circulation of the oxygen deficiency zone in the eastern tropical South Pacific Ocean

The distribution of current bands at 86° W shows the currents responsible for oxygen supply by eastward flow into the OMZ and westward transport of oxygen-poor water by westward current bands. The direct velocity distribution along about 86° W (Fig. 2) shows the typical equatorial current bands like the EUC, SICC, SEIC, SSCC and the SECC. However, there are differences compared to the regular situation. In the eastern Pacific typically the SSCC core is located in the density range 26.2–26.5 kg m^{-3} around 6° S (e.g. Stramma et al., 2010) with a weak but consistent secondary SSCC poleward of the SSCC and extending to greater densities (Rowe et al., 2000). In November 2012, however, the sSSCC was stronger than the SSCC especially in the density range 26.2–26.5 kg m^{-3} while the SSCC was very weak (Fig. 2). Both SSCC bands showed an unusually strong eastward component in the depth range 400 to 700 m.

The Galapagos Islands form a 135 km wide barrier to the EUC straddling the equator at 91.66° W. Here the EUC bifurcates into a shallower/southern core EUCs and a deeper/northern core EUCd (Karnauskas et al., 2010). Mooring observations at the

OSD
11, 2205–2243, 2014

equator at 110, 95 and 85° W showed a strong EUC signal with a core above 100 m depth in February 1982 at 110 and 95° W and at 150 m depth in November 1981 at 85° W (Karnauskas et al., 2010; Fig. 1). Our ADCP measurements in November 2012 show the core of the EUCd even deeper at about 250 m depth, while the EUCs is missing at the equator, but may be shifted southward to 3–4° S in the upper 100 m (Fig. 2) as a flow that deflects southeastward toward the coast of Peru (Karnauskas et al., 2010). The EUCd is connected to the SICC, with the isopycnal 26.65 kg m^{-3} as boundary between these two current bands. With the strong EUCd the EIC is not visible in November 2012, but only a reduced eastward flow component is seen at about 400 m depth north of the SICC near the equator.

South of 15° S the velocities are predominantly westward, showing the northern part of the South Pacific subtropical gyre. Overlain on this westward flow are the signatures of two shallow cyclonic features at about 23.5 and 18° S and a deeper reaching anticyclonic feature at about 22° S (Fig. 2), which are also visible in the sea level height anomaly (Fig. 1).

In March 1993 and in February 2009 the eastward flow of the EUC at 85°50′ W was observed completely in the upper 200 m between 2° S and 2° N. The EUC at 85°50′ W between 2° S and 2° N in the upper 200 m in March 1993 was 16.3 Sv while in February 2009 it was only 4.9 Sv from the ADCP measurements. The observed EUC at 85°50′ W in the box 2° S to 2° N in the upper 200 m is 7.2 Sv for November 2012; however, as described above, at that time part of the EUC transport was at deeper depth. Based on observations at 95° W, a strong EUC season was defined for March to July but a weak EUC in October to December (Karnauskas et al., 2010). However, results from a climate model for 110° W (Cravatte et al., 2007) show a strong EUC for April to June and a stronger EUC for October to December than for February. Hence, the stronger EUC at the end of March 1993 compared to mid-February 2009 is in agreement with the Karnauskas et al. (2010) results, while the enhanced deep EUC in November 2012 compared to mid-February 2009 is in agreement to the Cravatte et al. (2007) results and show the influence of the seasonal signal on the EUC.

OSD
11, 2205–2243, 2014

The circulation at different depths off Peru in November/December 2012 from ADCP measurements, color-coded with the oxygen of adjacent CTD-oxygen profiles, shows the transport paths of oxygen rich water towards the OMZs in the equatorial region (Fig. 3) below the surface layer. At 50 m depth (Fig. 3a) the lowest CARS-climatological oxygen is located at the equatorial channel and near the South American continent due to equatorial and coastal upwelling. The direct observations in November 2012 show deviations from the climatological mean, e.g. an eastward flowing current at about 3–4° S and the upper reaches of the sSSCC at about 9° S supply oxygen-rich water to the eastern Pacific. Near the shelf oxygen poor water is transported alongshore at 50 m depth with northwestward as well as southeastward flow components. At 16° S high oxygen values at 50 m depth are related to the anticyclonic eddy located at the shelf break at the end of 2012 (Stramma et al., 2013).

In the upper OMZ at 200 m depth (Fig. 3b) the low oxygen core is centered at about 12° S and reaches from the southern Peruvian coast into the open ocean. The direct observations agree with the low CARS-oxygen distribution in the center of the OMZ. The highest oxygen concentration in 200 m depth is observed in the southwest in the northern reaches of the South Pacific subtropical gyre, connected to a broad westward flow component. Near the equator, eastward supply of oxygen by eastward flow also agrees to the climatological oxygen distribution. At the 6° S section the northward flow component carries oxygen-poor water to the north. At the 16°45′ S section the westward flow with low oxygen water reaches further west than the climatological mean. The anticyclonic eddy at 16° S is slightly lower in oxygen than the CARS-climatology and exhibits the reduced oxygen distribution in the eddy at 200 m depth.

The core of the OMZ is located at about 375 m depth. The direct velocity and oxygen observations show even lower oxygen values than expected from the climatological mean (Fig. 3c) with less than 10 µmol kg^{-1} in almost the entire measurement region including the equatorial channel; the only exception is the subtropical gyre in the southwest. Even the eastward flowing SICC north of 4° S transports low oxygen compared

OSD
11, 2205–2243, 2014

to the CARS climatology eastward. At 16°45′ S near the shelf, the low oxygen and the anticyclonic circulation is related to the strong anticyclonic mode water eddy.

The lower part of the OMZ at 600 m depth (Fig. 3d) shows the low oxygen layer restricted in the eastern South Pacific to the region from 5 to 13° S. Near the equator there is again eastward oxygen supply by the lower part of NICC and SICC. In most locations the November/December 2012 flow field agrees with the climatology. The westward SEC at 10–12° S is located a bit more south transporting low oxygen water westward and again the westward flow at 16°45′ S with low oxygen water reaches further south than in the climatological mean.

The velocity distribution on the sections off the Peruvian coast in November and December 2012 (see Fig. 1) shows the southeastward flowing PCUC with variable structure and strength (Fig. 4). The transports for the depth layer 25 to 500 m up to 200 km off the coast are −1.0 Sv at 5° S, −2.3 Sv at 7° S, −0.9 Sv at 9° S, −1.1 Sv at 10° S, −3.9 Sv at 11° S, −0.5 Sv at 13° S, −2.5 Sv at 14° S and −0.8 Sv at 16° S. At 5° S the core of the PCUC is located west of the shelf break probably due to the contribution of the southern band of the EUC (Chaigneau et al., 2013; their Fig. 1). At 7, 9 and 10° S the PCUC is attached to the shelf. At 11° S the maximum transport of −3.9 Sv is reached, with one current core at the shelf and a second one offshore with water from the SSCC. At 13 and 14° S the PCUC near the shelf weakens due to a deep equatorward current flowing below the PCUC and referred to as Chile-Peru Deep Coastal Current by Chaigneau et al. (2013). At 16° S the PCUC is weak with only 0.8 Sv, as at that time a strong anticyclonic mode water eddy was located at the shelf (Stramma et al., 2013) with a strong northwestward flow component. The region near the shelf north of 15° S has an eddy frequency of about 20 to 30 % while south of 15° S it has an eddy frequency of up to 50 % (Chaigneau et al., 2008); hence, the PCUC is disturbed by eddies mainly in the southern region of Peru. The mean alongshore southeastward transport of the 8 sections between 5 and 16° S is 1.6 Sv and agrees to the 1.6 ± 0.4 Sv from long-term measurements between 7 and 13° S (Chaigneau et al., 2013). Between 13 and 9° S an equatorward flow in the upper 100 m is seen which could be part of the

OSD
11, 2205–2243, 2014

Peru Coastal Current, seen in the same geographical region at 25 m depth in the mean flow field (Chaigneau et al., 2013; their Fig. 3).

3.2 Float measurements

The nine floats deployed with a parking depth at 400 dbar provide information on the long term spreading and variability at about 400 m depth. The floats provided data for time periods between 710 and 1780 days (Fig. 5). The floats deployed at 2, 4° S and 6° S all moved fast westward within the equatorial current system. The fastest westward velocity with a mean northwest flow of 4.2 cm s^{-1} was that of the float deployed at 2° S, which entered the EIC and moved fast westward, before it left the EIC at 115° W and moved northward. The floats deployed at 4 and 6° S moved westward within the SEIC north of 5° S and the float deployed at 4° S shifted into the eastward flowing SSCC at about 108° W and moved back to 93° W before shifting again into the SEIC. As can be seen from the mean oxygen distribution at 400 m depth the SEIC carries the tongue of low oxygen far westward. The floats deployed at 8 and 10° S were located in a stagnant flow region (Czeschel et al., 2011) and moved slowly with less than 1 cm s^{-1} in the mean to the south.

The floats with a parking depth at 400 dbar deployed in April 2011 along 20° S are in the transition region between the OMZ and the well oxygenated subtropical gyre. These floats are strongly influenced by eddies which is reflected in the float paths (Fig. 5). Three of the floats moved slowly (~ 1 cm s^{-1}) westward with a slight southward component for the two floats east of 80° W, while one float entered the Peru Coastal Current and was transported northwestward.

Profiling floats sometimes are trapped for some time in eddies. Floats equipped with oxygen sensors are able to register the water mass and oxygen changes of an eddy when trapped in an eddy. A float with oxygen sensor (float 3900715) deployed on 26 October 2008 at 20.1° S, 85.6° W had a lifetime of only 1.5 years, nevertheless it stayed for more than half a year in a cyclonic eddy (Fig. 6). The float path shows two cyclonic loops (Fig. 6a), which lead to an up-rise of the low oxygen layer in the upper

OSD
11, 2205–2243, 2014

ocean (Fig. 6b). The strongest oxygen anomaly is located at about 300 m depth and the density, salinity, temperature and oxygen time series were plotted at 300 m depth. The 450 to 250 m geopotential anomaly (Fig. 6c) shows a strong decrease from late March to September 2009. The SSHA anomaly was extracted from the daily-delayed time product at the float location and the SSHA shows very good agreement to the geopotential anomaly at the subsurface layer. The animation of the float location relative to the SSHA (Supplementary movie F1) shows the cyclonic movement. At the beginning of the float mission the float crosses a regular anticyclonic eddy before it completes two full loops around the strong cyclonic eddy. As the cyclonic eddy moves westward, the cyclonic loops are better visible in the movie than in the flow path figure (Fig. 6a). Due to the uprise of the isopycnals in cyclonic eddies the density at 300 m increases, in connection with a salinity increase, a temperature decrease and an oxygen decrease at 300 m depth (Fig. 6d–f). The flow path at the end of the cyclonic eddy influence looks like an anticyclonic movement, however inspection of the satellite data showed that the float moved southward at the boundary of the cyclonic eddy before it was entering an anticyclonic eddy in October 2009, visible in the low oxygen layer located at 350 m depth.

Float 3900729 deployed on 18 November 2008 at 19.0° S, 79.6° W had a lifetime of more than 5 years, and stayed during that time between 78 and 86° W (Fig. 7a). The oxygen time series shows several events where the oxygen below the mixed layer decreases and the low oxygen layer extends vertically. This is the signature of anticyclonic eddies. Anticyclonic eddies in the region off Peru show the main anomalies at deeper depths than cyclonic eddies (Chaigneau et al., 2011); thus, the anomalies for float 3900729 are presented at 350 m depth. In late 2009 and early 2010, two cyclonic eddies crossed the float path and these cyclonic eddies are seen because of their increasing oxygen layers (Fig. 7b), low 450–250 m geopotential anomaly and higher density, lower salinity, lower temperature and higher oxygen at 350 m depth (Fig. 7c–g). In mid-2012 and early 2013 two anticyclonic mode water eddies crossed the float path, visible as a vertically upward and downward extended low oxygen layer (Fig. 7b).

OSD
11, 2205–2243, 2014

These mode water eddies show high 450–250 m geopotential anomaly and at 350 m depth lower density, higher salinity, higher temperature and lower oxygen (Fig. 7c–g).

Floats with oxygen sensors active for several years cover several annual cycles of the mixed-layer and the near surface layer. From a float near Hawaii and from a float in the central South Pacific it was found that mixing events during early winter homogenize the upper water column and cause low oxygen concentrations. Oxygen then increases below the mixed layer at a nearly constant rate. This continuous oxygen increase is consistent with an ecosystem that is a net producer of fixed carbon throughout the year, with episodic events not required to sustain positive oxygen production (Riser and Johnson, 2008). Net community production (NCP), which is equal to primary production minus respiration at all trophic levels, is difficult to measure. The balance of oxygen production and consumption by using the oxygen sensors on the floats led to highest NCP of about 15 mmol C m^{-3} yr^{-1} near Hawaii and about 7 mmol C m^{-3} yr^{-1} in the South Pacific gyre (Riser and Johnson, 2008). Here we use the same method as described by Riser and Johnson (2008) to derive the NCP from a float track located in the eastern South Pacific. The float 3900727 was deployed on 11 November 2008 at 19° S, 78.7° W (Fig. 8a) and moved northwestward for more than 5 years. The time-series of density, salinity, temperature, and oxygen (Fig. 8b–e) clearly show the annual cycles. Periods of convective overturn in the upper 150 m during which density, salinity, temperature and oxygen become vertically homogenous are present near the end of each year in response to the annual cycle of surface heat flux (Mechoso et al., 2014). Oxygen concentrations reach vertically uniform values during this period. In between the convective overturn oxygen accumulates in the water trapped under the seasonal thermocline and produces a distinctive shallow oxygen maximum (Fig. 8e).

The annual cycle of oxygen concentration in 64 m depth for the period 17 November 2008 to 16 November 2013 shows a continuous increase with time in the shallow oxygen maximum layer from mid-May to early April (Fig. 9e). The oxygen increase between mid-May and mid-November within the mixed layer correlates with a salinity and temperature decrease (Fig. 9c and d) and can be produced by changes in solubility by

OSD
11, 2205–2243, 2014

mixing in the mixed layer. Whereas the oxygen concentration increase between mid-November and early April below the mixed layer cannot be driven by oxygen solubility changes, which shows in fact a decrease during that period (Fig. 9e), and as the float moves horizontally with the water parcels must be caused by biological oxygen production.

The rate of oxygen production was determined after Riser and Johnson (2008) from the slope of a straight line that fits the oxygen data best in a least square sense against time for the whole period of oxygen increase from mid-May to early April (about 320 days, Fig. 10a). This period is estimated from the maximum oxygen increase between 40 to 80 m depth. The oxygen increase from the slope of the time series for all depths is then converted into carbon uptake with the modified Redfield ratio (150 mol of O_2 produced per 106 mol of CO_2 fixed, Anderson, 1995). The daily increase is extrapolated to an annual rate of the NCP which is highest in 58 m depth with a rate of $16.7 \pm 6\,\mathrm{mmol\,C\,m^{-3}\,yr^{-1}}$ (Fig. 10c). NCP estimates from a float in the South Pacific gyre (Riser and Johnson, 2008) determined from the slope of the annual cycle of oxygen against time for the period from June to May show highest values of $8.5 \pm 5\,\mathrm{mmol\,C\,m^{-3}\,yr^{-1}}$ in 87 m depth which is smaller than the value calculated from the data of the float propagating along the OMZ boundary.

In the upper 58 m the NCP is derived from the slope of oxygen anomaly (oxygen minus oxygen solubility) against time in the mixed layer showing their highest values of $12.6 \pm 4.9\,\mathrm{mmol\,C\,m^{-3}\,yr^{-1}}$ in 48 m depth. The NCP from the slope of oxygen anomaly against time within the mixed layer in the South Pacific also shows smaller rates with a maximum of 10 ± 1.3 in $\mathrm{mmol\,C\,m^{-3}\,yr^{-1}}$ in 87 m depth.

NCP rates determined from oxygen above the pycnocline can be imprecise due to oxygen loss to the atmosphere by gas exchange. Therefore the rate of oxygen production is determined from the slope of oxygen increase against time strictly below the mixed layer to avoid oxygen changes due to solubility variations. The periods of oxygen increase depend on the depth of the mixed layer (Fig. 10b). Due to lack of net community production the NCP calculation for the period November 2009 to April 2010

OSD
11, 2205–2243, 2014

was skipped. The NCP is highest in 64 m depth with a rate of 7.7 ± 3.2 mmol C m^{-3} yr^{-1} (Fig. 10c) with a strong oxygen increase between end of November to early April.

3.3 Changes on the 86° W repeat section

The oxygen changes between March 1993 and November 2012 along the 86° W section (Fig. 11) show regions of increase as well as decrease between these two cruises. In the equatorial channel between 2° N and 5° S, changes in oxygen similar to those seen between February 2009 and March 1993 on the same section (Czeschel et al., 2012; Fig. 7f) are present: a decrease of oxygen in the upper 400 m and an oxygen increase between 400 and 800 m depth. In the core of the oxygen minimum zone between 5 and 18° S there is mainly a weak oxygen increase between the March 1993 and the November 2012 cruise, with a region of oxygen decrease at 100 to 200 m depth and at mid-depth at 11 to 13° S. The reversal between oxygen decrease and oxygen increase south of 18° S is related to the eddy activity in this region as can be seen in satellite sea level height anomaly (Fig. 1).

The oxygen increase in the region north of 18° S might be related to the El Niño status. For the eastern Pacific, the Niño1+2 index defined as the temperature anomaly for the area 0 to 10° S, 80–90° W is most relevant. The monthly Nino1+2 indices (http://www.cpc.ncep.noaa.gov/data/indices/sstoi.indices) show for March 1993 +0.65, for April 1993 +0.97, for February 2009 −0.11, and for November 2012 −0.38. A comparison with an extended optimum multi-parameter analysis between the sections in March 1993 and February 2009 showed that during a cold phase the heave of relatively oxygen-rich Antarctic Intermediate Water into the depth range 150 to 500 m leads to higher oxygen values in the upper ocean (Llanillo et al., 2013). As the Niño1+2 index shows an even larger cold phase for November 2012 compared to February 2009, the oxygen increase north of 18° S seems to be caused by the El Niño phase differences. As a consequence, the comparison in oxygen changes between single ship sections

OSD
11, 2205–2243, 2014

has to be interpreted with great care taking El Niño phases and eddies as well as seasonal signals into account.

The Interdecadal Pacific Oscillation (IPO; Power et al., 1999) is the almost Pacific-wide manifestation of the Pacific Decadal Oscillation with as much variance in the Southern Hemisphere Pacific down to at least 55° S as in the Northern Hemisphere. Pronounced strengthening in Pacific trade winds over the past two decades has accounted for cooling of the tropical Pacific and slowing down the surface warming. Extra heat uptake has come about through increased subduction in the Pacific shallow overturning cells, enhancing heat convergence in the equatorial thermocline. At the same time, the accelerated trade winds have increased equatorial upwelling on the central and eastern Pacific, lowering sea surface temperature there (England et al., 2014). In the schematic figure for the trends in temperature and circulation between a positive IPO and a negative IPO between 1992 to 2011 (England et al., 2014, their Fig. 3), a negative temperature deviation and stronger westward flow anomalies are present in the upper 200 to 300 m in the eastern equatorial Pacific. The temperature differences along 85°50′ W between February 2009 and March 1993 show the proposed decrease in temperature in the upper 300 m near the equator (Fig. 12a) as well as a decrease in oxygen and a stronger relative westward flow component (Fig. 12b). As discussed before, the EUC shows a seasonal signal with stronger transports in late March than mid-February. However, measurements in late March 2009 resulted in a EUC flow of 7–11 Sv (Collins et al., 2013), hence less than the 16.3 Sv for late March 1993. But the fact that the velocity difference between February 2009 and March 1993 (Fig. 12b) is not only restricted to the EUC but also to the region north of 5° S points to a larger scale decrease in the velocity field. Hence, the difference in temperature and the velocity component between 1993 and 2009 is in agreement to the proposed intensification of wind-driven circulation in the Pacific and the ongoing warming hiatus (England et al., 2014). The strong positive temperature anomaly near 9° S in the upper 100 m and negative anomaly in 100 to 600 m depth is caused by a mode water eddy located on the section in 1993.

OSD
11, 2205–2243, 2014

3.4 Nutrient changes

Redfield et al. (1963) were the first to notice that the ratio of elements in seawater is remarkably similar to that of living and dead biomass, namely the ratios ($P : N : C : O_2$) are 1 : 16 : 106 : 138. Oxidation of biological debris leads to an increase of phosphate (PO_4), nitrate (NO_3) and carbon dioxide (CO_2) while oxygen is consumed. Different Redfield ratios were discussed later, e.g. Peng and Broecker (1987) described an $-O_2/P$ ratio near 175. Recently, in a study stratifying oxygen, nitrate and phosphate with respect to potential temperature to account for the strong dependence of oxygen saturation on temperature, clear regression lines emerged between oxygen and nitrate/phosphate that were found to be close to the original Redfield ratio (Ishizu and Richards, 2013).

In the subarctic Pacific Ocean, nutrient enrichment in nitrate, phosphate and silicate has been observed since the mid-1980s while oxygen decreased (Whitney et al., 2013). Nutrient measurements in the open tropical and South Pacific Ocean are sparse. Oxygen trends at about 86° W were computed since 1976 for the upper 700 m from existing historical data and the *Meteor* cruise in February 2009 (Czeschel et al., 2012). For the region along the November 2012 cruise track we checked the availability of nutrient data in the historical data base. In the regions 2° N to 2° S, 2 to 5° S and 5 to 8° S it was possible to compute the oxygen and nutrient trends. South of 8° S historical data are too sparse along the cruise track to compute nutrient trends. As historical nutrient measurements are focused on the upper ocean and as the nutrient changes will have the largest impact on the biology in the upper ocean, the trends since 1976 were computed for the three equatorial areas for the layer 50 to 300 m (Table 1). The area 2° N to 2° S represents the region of the eastward flowing EUC, 2 to 5° S the westward flowing SEC/SEIC region and 5 to 8° S the eastward flowing SSCC region.

The oxygen trend for all three areas is negative and significant with slightly more than 1 $\mu mol\,kg^{-1}\,yr^{-1}$. Floats with oxygen sensors deployed in the investigation area confirm the oxygen trend derived from the *Meteor* stations sampled in February 2009

OSD
11, 2205–2243, 2014

(Fig. 13a). Although only a few years were available for the nutrient trend computations, the positive trends for nitrate and phosphate are seen in all three areas and are significant within 95 % at 2° N–2° S and 2–5° S for nitrate and 2–5° S for phosphate (Fig. 13). Silicate trends are not significant and change from a positive trend between 2° N and 5° S to a negative trend at 5 to 8° S. Whitney et al. (2013) hypothesized that warming and oxygen loss in the subarctic Pacific pycnocline initiated a vertical redistribution of nutrients due to compression of vertical migrator habitat and/or changes in dissolution of sinking particles are responsible for the nutrient changes. Such processes could be also at work in the region of decreasing oxygen in the equatorial channel of the Pacific Ocean.

4 Discussion and conclusion

In this study the eastern tropical South Pacific off Peru was investigated from recent ship cruises, floats and historical hydrographic data. The oxygen and velocity distribution in November/December 2012 at different depth layers between 50 and 600 m depth indicated that the expected mean circulation of the tropical eastern South Pacific is modified by seasonal variability such as that of the EUC, which is known to show a seasonal signal, and by eddies on the poleward side of the OMZ. In November 2012 the Equatorial Undercurrent was centered at 250 m depth, deeper than in earlier observations and merged with the SICC. The shallow part of the EUC was absent or shifted southward to 3–4° S in the upper 100 m depth carrying relatively oxygen-rich water eastward at 50 m depth (Fig. 3a). The southeastward continuation of the equatorial water near the Peruvian shelf in the depth range 25 to 500 m within the Peru Chile Undercurrent in December 2012 showed a mean transport of 1.6 Sv and is in agreement to long-term ADCP measurements of the PCUC of 1.6 ± 0.4 Sv (Chaigneau et al., 2013). Chaigneau et al. (2013) state that the PCUC experiences relatively weak seasonal variability, hence the December 2012 transports agree very well with the mean PCUC transport.

OSD
11, 2205–2243, 2014

Float measurements turned out to be a useful tool for long-term surveys of the ocean, especially floats with oxygen sensors. The floats deployed with a parking depth at 400 m show fast westward flow in the equatorial channel, while none of the equatorial floats moved towards the South American continent. The floats deployed at 8° S and south of 8° S indicate sluggish flow in the OMZ. For a float which stayed in a cyclonic eddy for more than half a year, the SSHA was in good agreement with the subsurface geopotential anomaly (Fig. 6) and shows that cyclonic eddies are well visible in SSHA maps. From a float with oxygen sensor and a lifetime of more than 5 years drifting from about 20° S, 80° W to 16° S, 98° W it was possible to estimate the NCP with the highest NCP rate in 58 m depth extrapolated to an annual rate of 16.7 mmol C m^{-3} yr^{-1}. This computation is similar to the approach by Riser and Johnson (2008), who derived a maximum of 8 mmol C m^{-3} yr^{-1} for a float in the South Pacific at about 24° S, 120° W. However, when only the time period is used when the float stayed below the mixed layer the highest NCP was found at 64 m depth with 7.7 mmol C m^{-3} yr^{-1}. The higher annual rate in our easternmost float is related to the higher productivity in the eastern South Pacific, while the float in the central South Pacific operated in a region that is considered to have one of the lowest rates of primary production in the world ocean (Behrenfeld et al., 2005; Riser and Johnson, 2008).

Changes on repeat sections have to be considered with care, as the differences are influenced by the El Niño phase and seasonal changes. The observed difference in temperature and the velocity component in the tropical Pacific at 86° W between 1993 and 2009 is in agreement with the proposed intensification of wind-driven circulation in the Pacific, probably related to the IPO as suggested by England et al. (2014).

In the open tropical eastern South Pacific, historical data sets for oxygen and nutrients are sparse; however it was possible to compute oxygen and nutrient trends in three regions at about 86° W between 2° N and 8° S. These trends in the layer 50 to 300 m depth since 1976 show a decreasing oxygen trend related to increasing nitrate and phosphate trends. Similar oxygen and nutrient trends were reported for the subarctic Pacific Ocean (Whitney et al., 2013) and the California Current region (Bograd

OSD
11, 2205–2243, 2014

et al., 2014), however more detailed biological and chemical investigations are needed to understand the trends and changes in oxygen and in nutrients.

The core of the OMZ in the eastern tropical Pacific is located in a region of stagnant flow. In the equatorial region, zonal current bands with seasonal cycles are responsible for modifying the oxygen content of the OMZ. The equatorial water is transported poleward off the shelf with the PCUC. The seasonal cycle of the PCUC is weak (Chaigneau et al., 2013); however south of about 15° S, eddies disturb the eastern boundary flow field. On the poleward side of the OMZ the subtropical gyre forms the boundary of the OMZ and the oxygen content is modified in this region mainly by eddies. Variations on different time scales like seasonal changes, El Nino and IPO modify the parameter distribution in the ETSP and influence the trends observed in oxygen and nutrients. Profiling floats with oxygen sensors are a useful tool to extend the shipboard measurements for up to 5 years to investigate the eddy influence on the mean circulation, and these floats can provide additional information on net community production in the near surface layer. Investigations of the different time and space scales are necessary to better understand the parameter distribution and circulation and its changes in the ETSP.

The Supplement related to this article is available online at doi:10.5194/osd-11-2205-2014-supplement.

Acknowledgements. The Deutsche Forschungsgemeinschaft (DFG) provided support as part of the "Sonderforschungsbereich 754: Climate-Biogeochemistry Interactions in the Tropical Ocean, A5" (RC, LS). Additional support was provided through the German BMBF funded Project SOPRAN under FKZ 03F0662A (TF) and through the US NOAA Climate Program Office to the Woods Hole Oceanographic Institution (RAW). We thank G. Krahmann, M. Lohmann and T. Baustian for providing measurements and final processing of the various data sets presented. We thank participants in VOCALS for help in deploying profiling floats. The altimeter data were produced by Ssalto/Duacs and distributed by Aviso with support from Cnes. We thank the authorities of Peru for the permission to work in their territorial waters.

OSD
11, 2205–2243, 2014

References

Anderson, L. A.: On the hydrogen and oxygen content of marine phytoplankton, Deep-Sea Res. Pt. I, 42, 1675–1680, 1995.

Ayon, P., Criales-Hernandez, M. I., Schwamborn, R., and Hirche, H.-J.: Zooplankton research off Peru: a review, Prog. Oceanogr., 79, 238–255, 2008.

Behrenfeld, M. J., Boss, E., Siegel, D. A., and Shea, D. M.: Carbon-based ocean productivity and phytoplankton physiology from space. Glob. Biogeochem. Cy., 19, GB1006, doi:10.1029/2004GB002299, 2005.

Bograd, S. J., Pozo Buil, M., Di Lorenzo, E., Castro, C. G., Schroeder, I. D., Goericke, R., Anderson, C. R., Benitez-Nelson, C., and Whitney, F. A.: Changes in source waters to the Southern California Bight, Deep-Sea Res. Pt. II, online first, doi:10.1016/j.dsr2.2014.04.009, 2014.

Chaigneau, A., Gizolme, A., and Grados, C.: Mesoscale eddies off Peru in altimeter records: identification algorithms and eddy spatio-temporal patterns, Prog. Oceanogr., 79, 106–119, 2008.

Chaigneau, A., Le Texier, M., Eldin, G., Grados, C., and Pizarro, O.: Vertical structure of mesoscale eddies in the eastern South Pacific Ocean: a composite analysis from altimetry and Argo profiling floats, J. Geophys. Res., 116, C11025, doi:10.1029/2011JC007134, 2011.

Chaigneau, A., Dominguez, N., Eldin, G., Vasquez, I., Flores, R., Grados, C., and Echevin, V.: Near-coastal circulation in the northern Humboldt Current system from shipboard ADCP data, J. Geophys. Res., 118, 5251–5266, doi:10.1002/jgrc.20328, 2013.

Chelton, D. B., Schlax, M. G., and Samelson, R. M.: Global observations of nonlinear mesoscale eddies, Prog. Oceanogr., 91, 167–216, doi:10.1016/j.pocean.2011.01.002, 2011.

Collins, C., Mascarenhas, A., and Martinez, R.: Structure of ocean circulation between the Galápagos Islands and Ecuador, Adv. Geosci., 33, 3–12, doi:10.5194/adgeo-33-3-2013, 2013.

Cravatte, S., Madec, G., Izumo, T., Menkes, C., and Bozec, A.: Progress in the 3-D circulation of the eastern equatorial Pacific in a climate model, Ocean Model., 17, 28–48, doi:10.1016/j.ocemod.2006.11.003, 2007.

OSD
11, 2205–2243, 2014

Cravatte, S., Kessler, W. S., and Marin, F.: Intermediate zonal jets in the tropical Pacific Ocean observed by Argo floats, J. Phys. Oceanogr., 42, 1475–1485, doi:10.1175/JPO-D-11-0206.1, 2012.

Czeschel, R., Stramma, L., Schwarzkopf, F. U., Giese, B. J., Funk, A., and Karstensen, J.: Middepth circulation of the eastern tropical South Pacific and its link to the oxygen minimum zone, J. Geophys. Res., 116, C01015, doi:10.1029/2010JC006565, 2011.

Czeschel, R., Stramma, L., and Johnson, G. C.: Oxygen decreases and variability in the eastern equatorial Pacific, J. Geophys. Res., 117, C01019, doi:10.1029/2012JC008043, 2012.

Deutsch, C., Brix, H., Ito, T., Frenzel, H., and Thompson, L.: Climate-forced variability of ocean hypoxia, Science, 333, 336–339, doi:10.1126/science.1202422, 2011.

England, M. H., McGregor, S., Spence, P., Meehl, G. A., Timmermann, A., Cai, W., Sen Gupta, A., McPhaden, M. J., Purich, A., and Santoso, A.: Recent intensification of wind-driven circulation in the Pacific and the ongoing warming hiatus, Nature Climate Change, 4, 222–227, doi:10.1038/NCLIMATE2106, 2014.

Firing, E., Wijffels, S. E., and Hacker, P., Equatorial subthermocline currents across the Pacific, J. Geophys. Res., 103, 21413–21423, doi:10.1029/98JC01944, 1998.

Grasse, P., Stichel, T., Stumpf, R., Stramma, L., and Frank, M.: The distribution of neodymium isotopes and concentrations in the eastern equatorial Pacific: water mass advection vs. particle exchange, Earth Planet. Sc. Lett., 353–354, 198–207, 2012.

Hansen, H. P.: Determination of oxygen, in: Methods of Seawater Analysis, edited by: Grasshoff, K. K. and Ehrhardt, M., Wiley-VCH, Weinheim, 75–89, 1999.

Ishizu, M. and Richards, K. J.: Relationship between oxygen, nitrate, and phosphate in the world ocean based on potential temperature, J. Geophys. Res.-Oceans, 118, 3586–3594, doi:10.1002/jgrc.20249, 2013.

Karnauskas, K. B., Murtugudde, R., and Busalacchi, J.: Observing the Galapagos-EUC interaction: insights and challenges, J. Phys. Oceanogr., 40, 2768–2777, doi:10.1175/2010JPO4461.1, 2010.

Kessler, W. S.: The circulation of the eastern tropical Pacific: a review, Prog. Oceanogr., 89, 181–217, doi:10.1016/j.pocean.2006.03.009, 2006.

Klein, P. and Lapeyre, G.: The oceanic vertical pump induced by mesoscale and submesoscale turbulence, Annu. Rev. Mater. Sci., 1, 351–373, 2009.

Llanillo, P. J., Karstensen, J., Pelegrí, J. L., and Stramma, L.: Physical and biogeochemical forcing of oxygen and nitrate changes during El Niño/El Viejo and La Niña/La Vieja upper-

OSD
11, 2205–2243, 2014

ocean phases in the tropical eastern South Pacific along 86° W, Biogeosciences, 10, 6339–6355, doi:10.5194/bg-10-6339-2013, 2013.

McGillicuddy Jr., D. J., Anderson, L. A., Bates, N. R., Bibby, T., Buesseler, K. O., Carlson, C. A., Davis, C. S., Ewart, C., Falkowski, P. G., Goldthwait, S. A., Hansell, D. A., Jenkins, W. J., Johnson, R., Kosnyrev, V. K., Ledwell, J. R., Li, Q. P., Siegel, D. A., and Steinberg, D. K.: Eddy/wind interactions stimulate extraordinary mid-ocean plankton blooms, Science, 316, 1021–1026, 2007.

Mechoso, C. R., Wood, R., Weller, R., Bretherton, C. S., Clarke, A. D., Coe, H., Fairall, C., Farrar, J. T., Feingold, G., Garreaud, R., Grados, C., McWilliams, J., de Szoeke, S. P., Yuter, S. E., and Zuidema, P.: Ocean-Cloud-Atmosphere–Land Interactions in the Southeastern Pacific: the VOCALS Program, B. Am. Meteorol. Soc., 95, 357–375, doi:10.1175/BAMS-D-11-00246.1, 2014.

Peng, T. H. and Broecker, W. S.: C/P ratios in marine detritus, Global Biogeochem. Cy., 1, 155–161, 1987.

Power, S., Casey, T., Folland, C. K., Colman, A., and Mehta, V.: Inter-decadal modulation of the impact of ENSO on Australia, Clim. Dynam., 15, 319–323, 1999.

Redfield, A. C., Ketchum, B. H., and Richards, F. A.: The influence of organisms on the composition of sea water, in: The Sea, Vol. 2, edited by: Hill, M. N., Interscience, New York, 26–27, 1963.

Ridgway, K. R., Dunn, J. R., and Wilkin, J. L.: Ocean interpolation by four-dimensional least squares-Application to the waters around Australia, J. Atmos. Ocean. Tech., 19, 1357–1375, 2002.

Riser, S. C. and Johnson, K. S.: Net production of oxygen in the subtropical ocean, Nature, 451, 323–325, doi:10.1038/nature06441, 2008.

Rowe, D. G., Firing, E., and Johnson, G. C.: Pacific equatorial subsurface countercurrent velocity, transport and potential vorticity, J. Phys. Oceanogr., 30, 1172–1187, 2000.

Stramma, L., Johnson, G. C., Firing, E., and Schmidtko, S.: Eastern Pacific oxygen minimum zones: supply paths and multidecadal changes, J. Geophys. Res., 115, C09011, doi:10.1029/2009JC005976, 2010.

Stramma, L., Bange, H. W., Czeschel, R., Lorenzo, A., and Frank, M.: On the role of mesoscale eddies for the biological productivity and biogeochemistry in the eastern tropical Pacific Ocean off Peru, Biogeosciences, 10, 7293–7306, doi:10.5194/bg-10-7293-2013, 2013.

OSD
11, 2205–2243, 2014

Stramma, L., Weller, R. A., Czeschel, R., and Bigorre, S.: Eddies and an extreme water mass anomaly observed in the eastern South Pacific at the Stratus mooring, J. Geophys. Res. Oceans, 119, 1068–1083, doi:10.1002/2013JC009470, 2014.

Tatebe, H., Imada, Y., Mori, M., Kimoto, M., and Hasumi, H.: Control of decadal and bidecadal climate variability in the tropical Pacific by the off-equatorial South Pacific Ocean, J. Climate, 26, 6524–6534, doi:10.1175/JCLI-D-12-00137.1, 2013.

Ulloa, O., Canfield, D. E., DeLong, E. F., Letelier, R. M., and Stewart, F. J.: Microbial oceanography of anoxic oxygen minimum zones, P. Natl. Acad. Sci. USA, 109, 15996–16003, doi:10.1073/pnas.1205009109, 2012.

Whitney, F. A., Bograd, S. J., and Ono, T.: Nutrient enrichment of the subarctic Pacific Ocean pycnocline, Geophys. Res. Lett., 40, 2200–2205, doi:10.1002/grl.50439, 2013.

Winkler, L. W.: Bestimmung des im Wasser gelösten Sauerstoffs, Ber. Dtsch. Chem. Ges., 21, 2843–2855, 1888.

OSD
11, 2205–2243, 2014

Table 1. Linear trends in μmol kg^{-1} yr^{-1} with 95 % confidence intervals since 1976 in a 50 to 300 m layer for the ocean areas between 84 and 87° W for 2° N–2° S (Fig. 13), 2–5° S and 5–8° S. For phosphate at 2° N–2° S the years 1978 and 1979 and for silicate at 2–5° S the year 1976 were removed due to unrealistic low annual mean values. Trends not within the 95 % confidence interval are shown in brackets.

Parameter	2° N–2° S	2–5° S	5–8° S
Oxygen	−1.02 ± 0.49	−1.23 ± 0.67	−1.02 ± 0.84
Nitrate	+0.139 ± 0.112	+0.245 ± 0.165	(+0.101 ± 0.179)
Phosphate	(+0.0050 ± 0.0095)	+0.0110 ± 0.0087	(+0.0051 ± 0.0079)
Silicate	(+0.0461 ± 0.1880)	(+0.0127 ± 0.0734)	(−0.0483 ± 0.0699)

OSD
11, 2205–2243, 2014

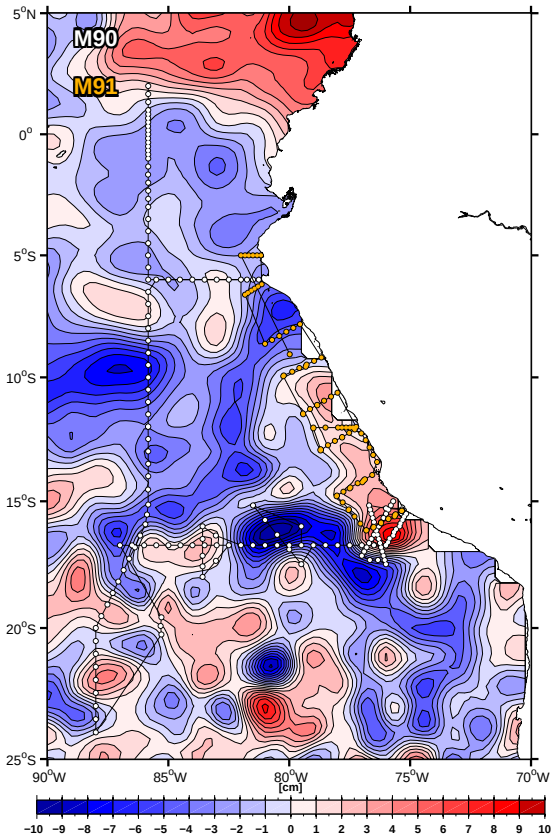

Figure 1. Aviso sea level height anomaly (in cm) for 21 November 2012, cyclonic features are shown in blue, anticyclonic ones in red. The cruise track (black line) and CTD stations (white and yellow dots) of R/V *Meteor* cruise M90 in November 2012 (white dots) and of cruise M91 in December 2012 (yellow dots) are included.

OSD
11, 2205–2243, 2014

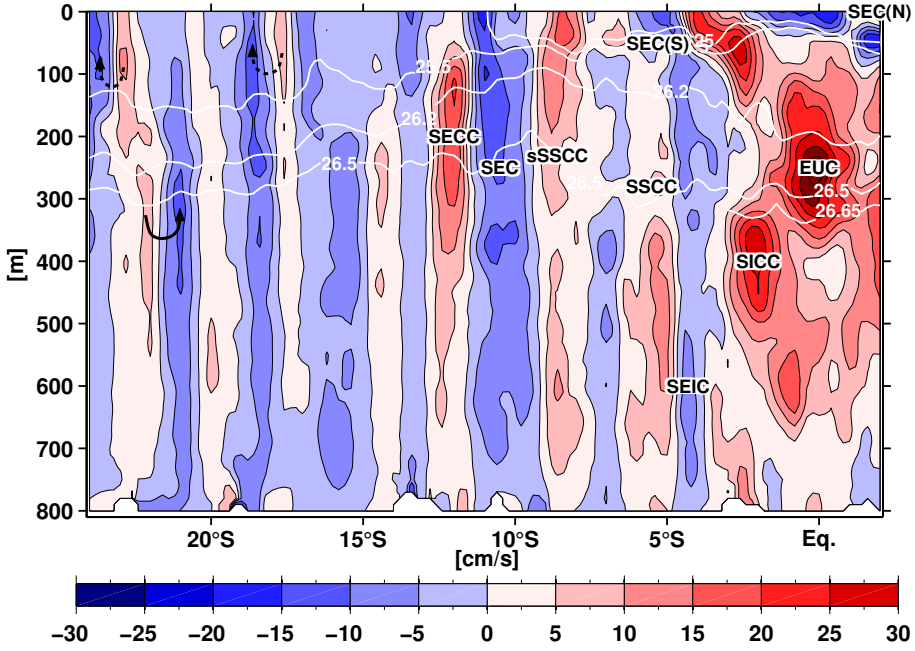

Figure 2. Zonal velocity distribution in cm s^{-1} (positive eastward) along about 86° W between 2° N and 24° S from the shipboard ADCP velocity data measured 1 to 13 November 2012. See text for indicated current bands. Some selected isopycnals are included as white lines. Cyclonic features at the southern part of the section are marked as dashed black arrows, an anticyclonic feature as solid black arrow.

OSD
11, 2205–2243, 2014

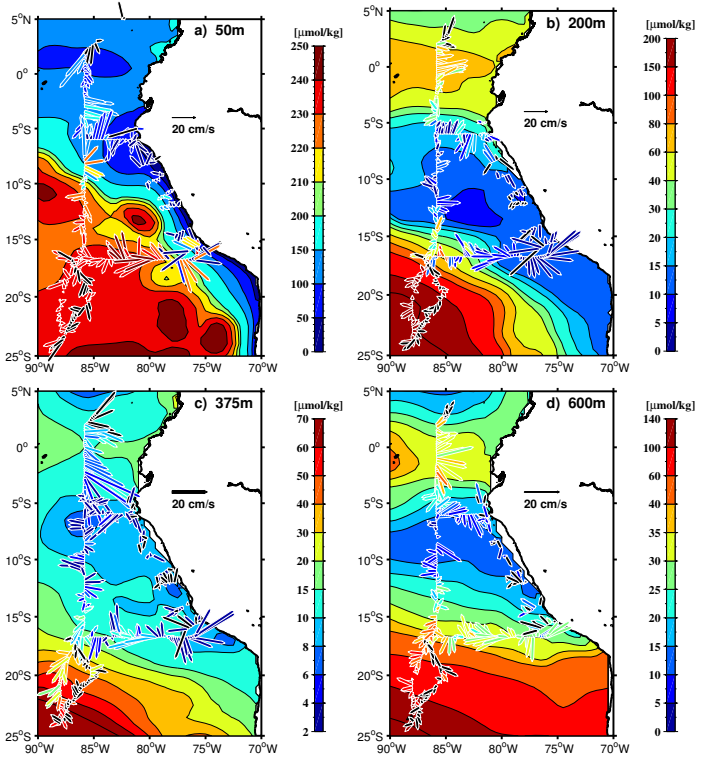

Figure 3. Horizontal distribution of ADCP velocity vectors at **(a)** 50 m, **(b)** 200 m, **(c)** 375 m and **(d)** 600 m depth recorded in November and December 2012 with current vectors colored with oxygen (in µmol kg^{-1}) of the accompanying CTD oxygen measurement at this depth. In case of no accompanying CTD oxygen measurement the current vectors are black. The oxygen distribution of the background field is from the CARS 2009 climatology (Ridgway et al., 2002) for November at 50, 200 and 375 m and the annual mean at 600 m depth. Please note the different color scales adjusted to fit the corresponding depth layer oxygen range.

OSD
11, 2205–2243, 2014

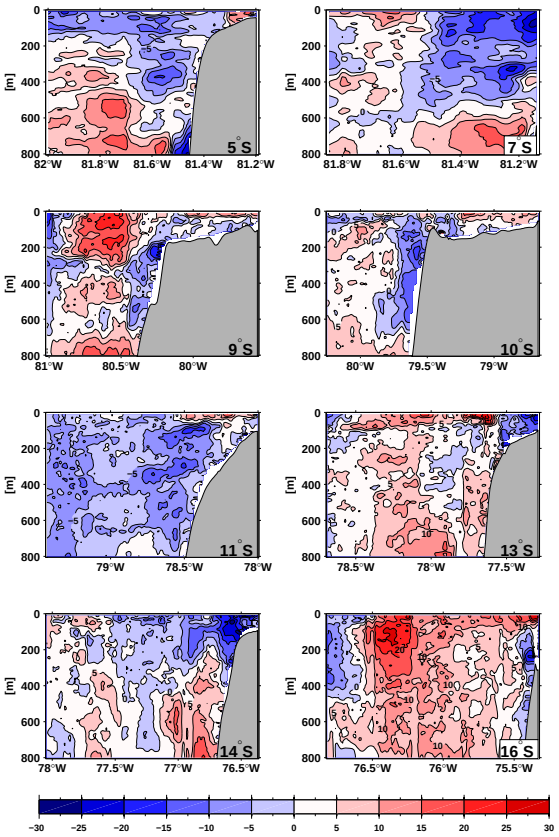

Figure 4. Cross-section velocity component parallel to the coast in cm s^{-1} (positive northwestward) for sections perpendicular to the coast near the Peruvian shelf (see Fig. 1) at about 16° S in November 2012 and 5, 7, 9, 10, 11, 13 and 14° S in December 2012.

OSD
11, 2205–2243, 2014

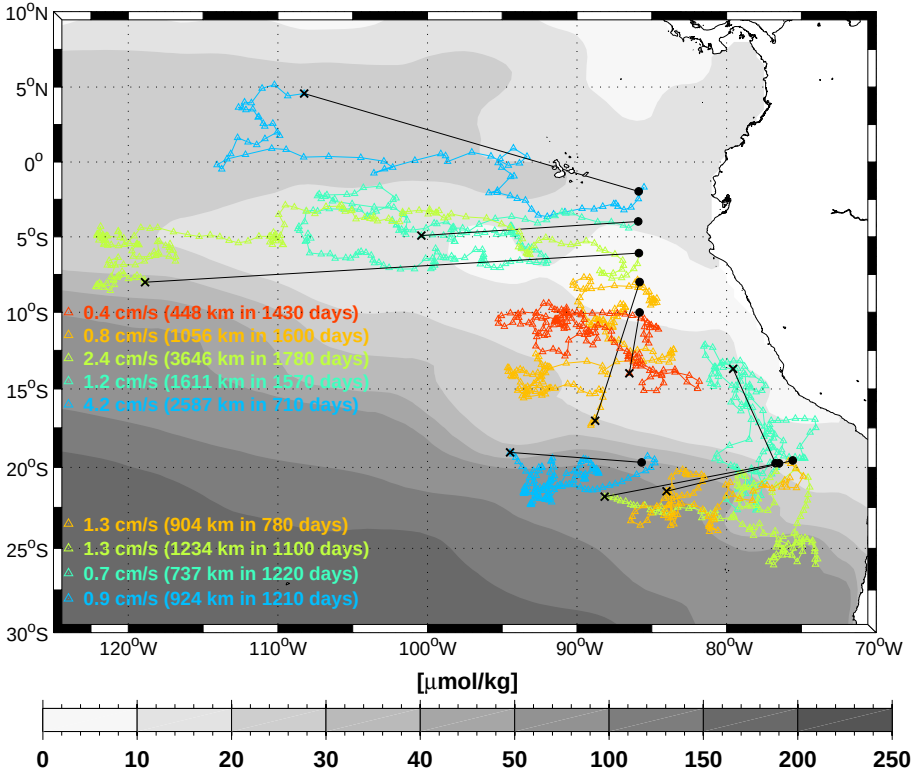

Figure 5. Floats drifting at 400 dbar deployed in February 2009 along 85°50′ W and in April 2011 along 20° S (in color) with mean velocity information for the entire lifetime of the floats or until August 2014 for floats which are still active. The symbols show the surfacing location every 10 days, the black line marks the connection between the deployment position and the last position used. Grey background field is the annual mean CARS 2009 (Ridgway et al., 2002) climatological oxygen distribution in µmol kg^{-1} at 400 m depth.

OSD
11, 2205–2243, 2014

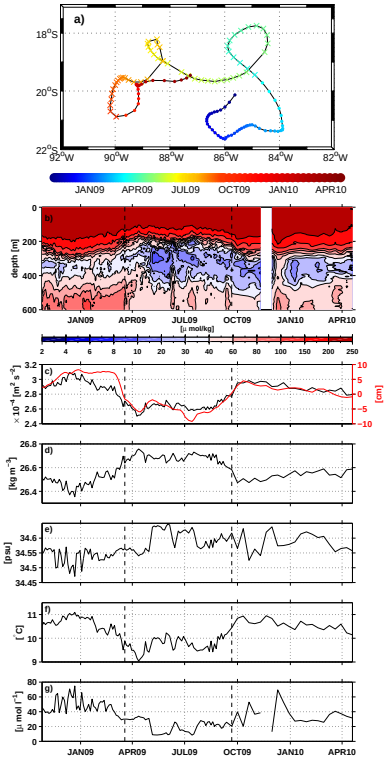

Figure 6. Measurements of float 3900715 in the tropical eastern South Pacific between 26 October 2008 and 19 April 2010 with **(a)** float path (color coded), **(b)** oxygen distribution vs. time in the upper 600 m, **(c)** geopotential anomaly (450 to 250 m, black curve) and SSHA from daily delayed-time satellite data at the float location (red curve), **(d)** density in 300 m depth, **(e)** salinity in 300 m, **(f)** temperature in 300 m, and **(g)** oxygen in 300 m. An erroneous oxygen profile in early November 2009 was removed. The float residence time of the float in the cyclonic eddy (19 March 2009 to 21 September 2009) is marked by X's **(a)** and dashed black lines **(b–g)**.

OSD
11, 2205–2243, 2014

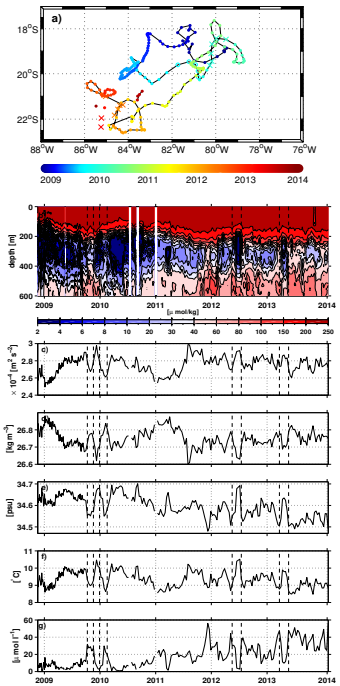

Figure 7. Measurements of float 3900729 in the tropical eastern South Pacific between 18 November 2008 and 6 February 2014 with **(a)** float path (color coded), **(b)** oxygen distribution vs. time in the upper 600 m, **(c)** geopotential anomaly (450 to 250 m), **(d)** density in 350 m depth, **(e)** salinity in 350 m, **(f)** temperature in 350 m, and **(g)** oxygen in 350 m. The residence time of the float in two cyclonic eddies (10 October to 19 November 2009, 29 December 2009 to 17 February 2010) and two anticyclonic mode water eddies (17 May to 16 July 2012, 23 March to 22 May 2013) is marked by X's **(a)** and dashed black lines **(b–g)**. In 2013 some profiles were recorded without the geographical location and only locations recorded are shown by dots or crosses not connected by a line.

OSD
11, 2205–2243, 2014

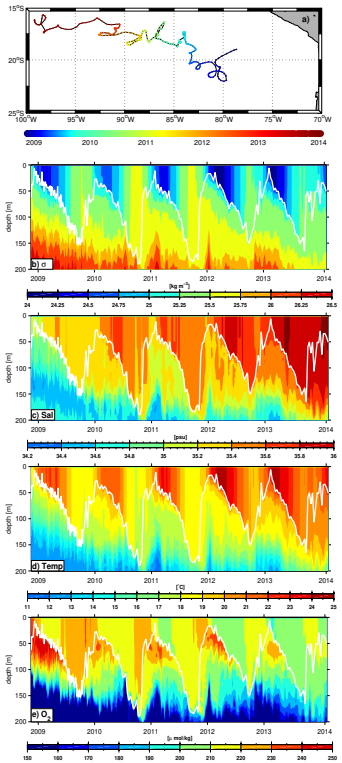

Figure 8. Measurements of float 3900727 in the tropical eastern South Pacific for the period 17 November 2008 to 11 February 2014 with **(a)** float path (color coded) and the distribution in the upper 200 m depth for **(b)** density, **(c)** salinity, **(d)** temperature, and **(e)** oxygen. The white curve in **(b–e)** is the mixed layer depth defined for the depth where the density is 0.125 kg m^{-3} larger than at the surface.

OSD
11, 2205–2243, 2014

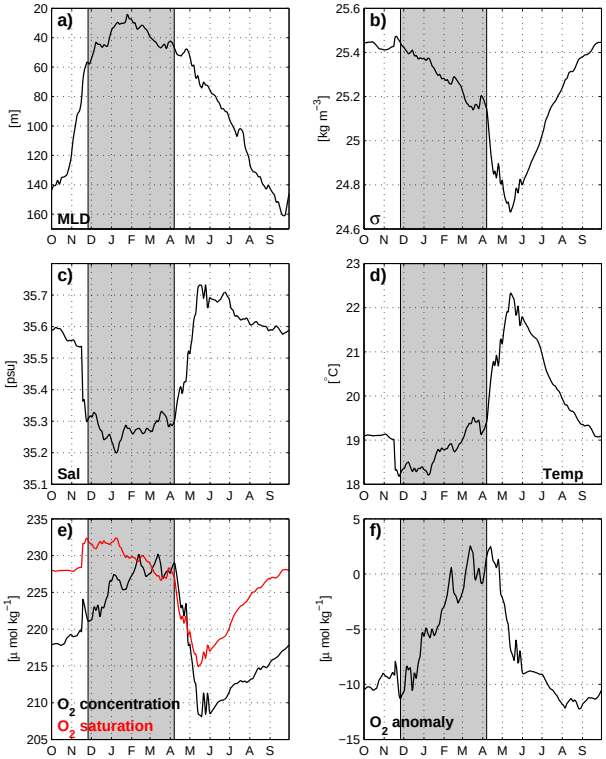

Figure 9. Mean annual cycle for the period 17 November 2008 to 16 November 2013 of float 3900727 in the tropical eastern South Pacific for **(a)** mixed layer depth (depth where the density is 0.125 kg m^{-3} larger than at the surface), and the distribution at 64 m depth for **(b)** density, **(c)** salinity, **(d)** temperature, **(e)** oxygen concentration (black curve) and oxygen saturation (red curve), and **(f)** oxygen anomaly (oxygen concentration minus oxygen solubility). Annual cycle plotted from October to end of September to follow the cycle of the mixed layer depth. The period of oxygen increase below the mixed layer between end November to early April is highlighted in grey.

OSD
11, 2205–2243, 2014

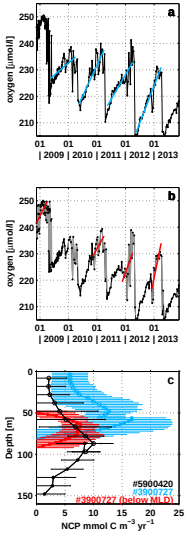

Figure 10. Oxygen concentration for float #3900727 at 58 m depth **(a)** and 64 m depth **(b)** shown as black lines and dots. Grey lines show the oxygen concentration below the mixed layer depth **(b)**. Blue **(a)** and red **(b)** lines are fitted to the oxygen increase each year for the period mid-May to early April **(a)** and for a period depending on the depth of the mixed layer **(b)**. Net community production (NCP, in mmol C m^{-3} yr^{-1}, **c**) for float WMO #5900420 (at 20° S to 22° S, 119° W to 128° W, as used in Riser and Johnson, 2008) with oxygen slope against time computed for the period mid-June to early May (black circles and dots) and for float 3900727 (see Fig. 8) with oxygen slope against time for the period mid-May to early April (blue circles and dots) both extrapolated for 365 days. NCP calculated only below the mixed layer depth for float 3900727 with variable periods (red dots). Open symbols were calculated from the slope of oxygen anomaly (oxygen – oxygen solubility) against time in the mixed layer. Solid symbols are an extrapolation to the surface of the highest rates based on the slope of oxygen against time at each site. Oxygen production was converted to carbon units using the modified Redfield ratio as in Riser and Johnson (2008). Error bars show the standard deviation of the NCP.

OSD
11, 2205–2243, 2014

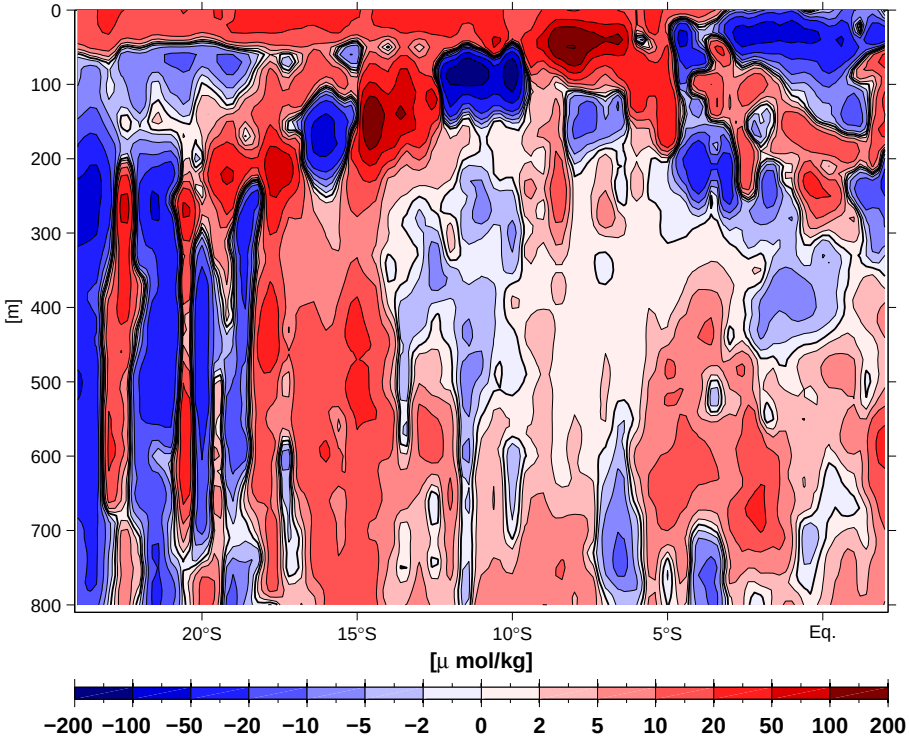

Figure 11. Oxygen differences along the section at about 86° W between November 2012 and March 1993.

OSD
11, 2205–2243, 2014

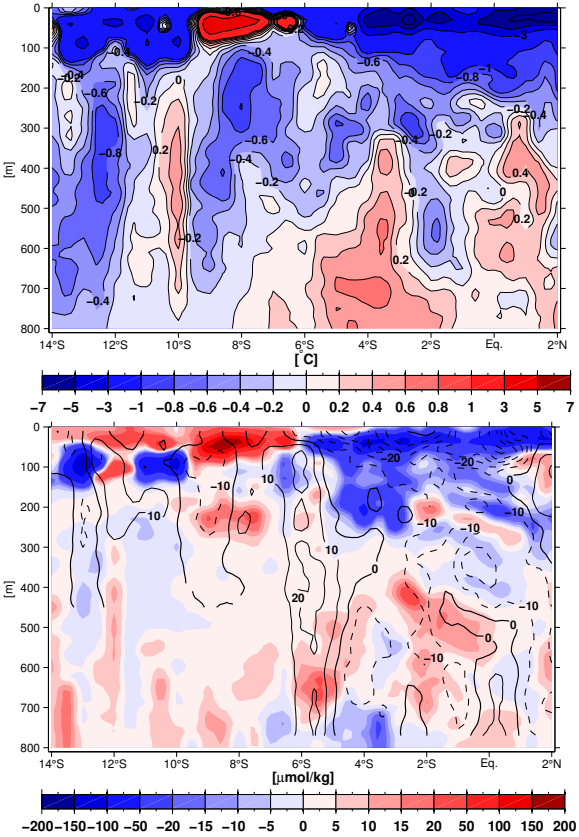

Figure 12. Distribution of differences along 85°50′ W between February 2009 and March 1993 in (top) temperature in °C and (bottom) oxygen in µmol kg^{-1} (color) and ADCP measured zonal velocity (black contours, cm s^{-1}, positive eastward).

OSD
11, 2205–2243, 2014

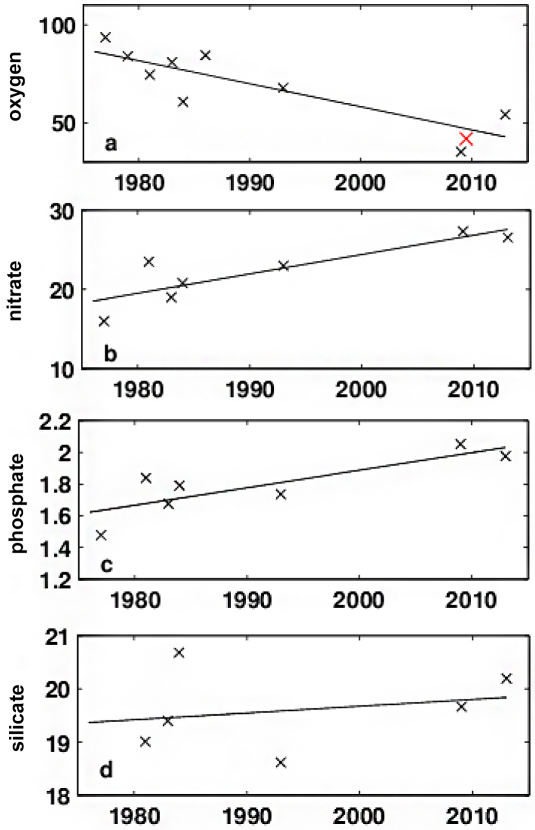

Figure 13. Trends since 1976 for the layer 50 to 300 m depth between 2° S and 5° S and 84° W and 87° W in µmol kg^{-1} yr^{-1} for **(a)** oxygen, **(b)** nitrate, **(c)** phosphate, and **(d)** silicate. For silicate the year 1976 was removed due to an unrealistic mean value (14.9 µmol kg^{-1} yr^{-1}). The red cross in **(a)** is the mean oxygen value for 2009 from profiling floats with oxygen sensors which provided profiles in the investigation area.

OSD
11, 2205–2243, 2014